



**Quantum Chemical Study on Gas Phase Decomposition
Pathways of Triethylgallane (TEG, Ga(C₂H₅)₃) and
Tertiarybutylphosphine (TBP, PH₂(t-C₄H₉)) under MOVPE
Conditions**

Journal:	<i>Physical Chemistry Chemical Physics</i>
Manuscript ID:	CP-ART-04-2014-001584.R1
Article Type:	Paper
Date Submitted by the Author:	20-Jun-2014
Complete List of Authors:	Stegmüller, Andreas; Philipps Universität Marburg, Fachbereich Chemie Rosenow, Phil; Philipps Universität Marburg, Fachbereich Chemie Tonner, Ralf; Philipps Universität Marburg, Fachbereich Chemie

SCHOLARONE™
Manuscripts

Quantum Chemical Study on Gas Phase Decomposition
Pathways of Triethylgallane (TEG, $\text{Ga}(\text{C}_2\text{H}_5)_3$) and
Tertiarybutylphosphine (TBP, $\text{PH}_2(t\text{-C}_4\text{H}_9)$) under MOVPE
Conditions

Andreas Stegmüller, Phil Rosenow, Ralf Tonner*

Keywords

Ab initio calculations, density functional calculations, gas-phase reactions, transition states, metal-organic vapour phase epitaxy

A. Stegmüller, P. Rosenow, Dr. R. Tonner

Fachbereich Chemie and Materials Sciences Center

Philipps-Universität Marburg

Hans-Meerwein-Strasse

35032 Marburg, Germany

corresponding author: tonner@chemie.uni-marburg.de

Abstract

The gas phase decomposition reactions of precursor molecules relevant for metal-organic vapour phase epitaxy (MOVPE) of semiconductor thin films are investigated by computational methods on the density-functional as well as on the ab initio (MP2, CCSD(T)) level. A comprehensive reaction catalogue of uni- and bimolecular reactions is presented for triethylgallium (TEG) as well as tertiarybutylphosphine (TBP) containing thermodynamic data together with transition state energies. From these energies it can be concluded that TEG is decomposing in the gas phase under MOVPE conditions ($T = 400 - 675$ °C, $p = 0.05$ atm) towards GaH_3 via a series of β -hydride elimination reactions. For elevated temperatures, further decomposition to GaH is thermodynamically accessible. In case of TBP, the original precursor molecule will be most abundant since all reaction channels exhibit either large barriers or unfavorable thermodynamics. Dispersion-corrected density functional calculations (PBE-D3) provide an accurate description of the reactions investigated in comparison to high level CCSD(T) calculations serving as benchmark values.

1 Introduction

Semiconductor materials composed of group 13 and group 15 elements (aka. III/V materials) grown on silicon surfaces have potential applications as highly efficient solar cells and lasers.[1] "Silicon photonics" aims at the combination of optical data processes with Si-based microelectronics technology, but is hampered by the indirect band gap of silicon and thus optically active overlayers have to be formed.[2] Those materials are often deposited onto silicon substrates in a vapor phase epitaxy procedure from metal-organic precursor molecules (MOVPE). In order to tune the materials towards direct optical gaps, metastable quaternary group III/V materials were developed which exhibit lattice constants close to the Si bulk value.[3] However, those materials can be grown quasi-epitaxially on Si(001) applying a 40-50 nm buffer layer of GaP.[4,5] The quality of the III/V material's optoelectronic properties is highly dependent on the structural quality of the GaP nucleation layer which goes hand in hand with the cleanliness of the Si substrate surface, choice and purity of the precursors and the specific suitability of the applied growth conditions.[6] Crystal defects can be propagated by mechanical strain caused by the hetero-layers' lattice mismatch or different thermal expansion coefficients. On the other hand, non-ideal reactor conditions lead to incomplete precursor decompositions and undesirable doping defects, e.g. carbon incorporation.[7] It is the declared goal of material scientists to minimize those defects during growth of promising III/V materials. Therefore, a detailed understanding of the chemical processes within the reactor is crucial and computational studies are used to complement experimental findings.[9-12] It is, for instance, difficult to obtain reaction-specific barriers from experiment (e.g. mass spectrometry) as detected species appearances can only be related to the overall temperature and reaction (growth) rate.[8,12,16]

One frequently applied precursor in the growth of III/V materials is trimethylgallane ($\text{Ga}(\text{CH}_3)_3$, TMG), which has a lower decomposition rate than triethylgallane ($\text{Ga}(\text{C}_2\text{H}_5)_3$, TEG) and pyrolyzes only at high temperatures (above 480 °C [16]) in the gas phase. Surface-assisted decomposition mechanisms, on the other hand, exhibit significantly lower barriers (<130 °C).[14] However, there is an increased tendency for carbon incorporation, because reactive and therefore uncontrollable radical species are formed from TMG, e.g. dimethylgallane and methyl radicals, which remain strongly bound to the Si surface.[12,14] By introducing ligands larger than methyl, decomposition temperatures (thermal barriers) were found to decrease: Tri-*tert*-butylgallane, e.g., undergoes clean decompositions via β -hydride eliminations already at 260 °C (low barrier of 160 kJ mol⁻¹ [15]) without carbon incorporation.[16] It has been found that this problem can be circumvented by using TEG as epitaxy precursor, which delivers GaN layers with high intensity photoluminescence and higher electron mobility than those grown with TMG.[17] Some pathways for TEG were investigated previously but no barriers were reported.[13,15] Low-barrier β -hydride

eliminations seem to play a major role for successful growth procedures and precursors with larger ligands were addressed by experimental and theoretical studies.[15,16,18]

As a common source for group 15 elements tertiarybutylarsine ($\text{AsH}_2(\text{t-C}_4\text{H}_9)$, TBA) and tertiarybutylphosphine ($\text{PH}_2(\text{t-C}_4\text{H}_9)$, TBP)[19a], are used as MOVPE precursors. Some decomposition pathways for TBP were computed in an early computational study on the HF level,[19b] supporting the suggestion of a breaking of the phosphorous-carbon bond in the initial step.[19c] A concise examination of decomposition pathways of TBP including barriers is not yet available. TEG and TBP fulfill general requirements for MOVPE precursor molecules such as lowered toxicity, suitable lab handling characteristics and, as investigated in this study, well-defined chemical stability.[9]

We want to briefly outline the experimental setup to set the stage for the computational investigations.[20] The original precursors are flushed into the reaction chamber in a hydrogen gas stream at 0.05 atm total pressure. TEG and TBP are kept separated in the gas phase by alternating the precursor flushes with pure hydrogen flushes, which rinses the reaction chamber. This procedure is referred to as flow-rate modulated epitaxy (FME) and was found to produce GaP layers of very high quality.[20] Hence, stable donor-acceptor complexes or oligomers of group 13 and 15 species, which have been extensively revised by Timoshkin and others [21-24], will presumably not be of major importance for the decomposition. The partial pressures of Ga and P precursors are very low so that the formation of elemental Ga or P clusters[26,27] can be neglected.

The aim of this study is now to investigate a comprehensive reaction catalogue for the important MOVPE precursors TEG and TBP in the hydrogen gas atmosphere via accurate computations on the DFT and ab initio level providing thermodynamic energies and barriers. To this end, 61 elementary reactions and reaction barriers for a rationally chosen subset of those were calculated on the MP2 and PBE-D3 level of approximation and checked against benchmark calculations on the CCSD(T) level. The presented decomposition catalogue covers four mechanism classes (homolytical bond cleavage, β -hydrogen decomposition, H_2 and alkane eliminations) for unimolecular reactions and three classes (radical recombination, H_2 and alkane eliminations) for bimolecular reactions with several reactants. Primarily, this study aims at revealing the resulting decomposition products from the gas phase. Secondly, it presents the chemical mechanisms of the most prominent decomposition classes, showing thermodynamic and kinetic trends for those reactions under experimental conditions. Thirdly, the accurate benchmark data allow an error estimation for production type DFT calculations. This will help both experimental and theoretical scientists to understand the specific decomposition behavior and tune reactor conditions towards clean and complete decompositions.

For the presented results some assumptions had to be formulated which include the

limitation of reactions with a maximum of two reaction partners (e.g. precursors + H₂), no agglomeration of multiple precursors of the same (due to low partial pressures) and of different types (due to separated input of Ga and P sources, respectively). Furthermore, reactor wall effects and the reactor layout are neglected in this study, however processes related to the substrate surface will be investigated in future studies.

2 Computational Details

Geometry optimizations without symmetry constraints were carried out using the Gaussian09 optimizer (standard convergence criteria)[30] combined with Turbomole (version 6.3.1) [31,32] energies and gradients (SCF convergence criterion 10^{-8} a.u., grid m4). Optimizations were carried out within the density functional approximation applying the GGA functional PBE[33] (widely used in materials science studies)[29,30] and on an ab initio level using the MP2 method. For the PBE calculations, dispersion effects were considered for the calculation of electronic reaction energies and molecular structure optimizations by applying the DFT-D3 method with an improved damping function (further called PBE-D3).[34,35]

One aim of this study is to establish a methodological standard for future studies on gas phase and surface chemistry in these systems. Therefore, the geometries and energies derived at the MP2 level were used as gas phase benchmark data for the PBE-D3 calculations of these molecular properties. Complementing the MP2 energies, CCSD(T) [36-39] energies of elementary reactions were derived based on MP2 geometries (on PBE-D3 geometries for transition states) to verify the accuracy of MP2 and PBE-D3. Minimum and transition state structures (the latter characterized by one imaginary mode) were confirmed by calculating the Hessian matrices on PBE-D3 (analytically [40]) and MP2 (numerically [41]). The reactants and products connected by a transition state were identified via an intrinsic reaction path (IRC) calculation. Thermodynamic corrections were subsequently derived by statistical thermodynamics in the double harmonic approximation under the assumption of no hindered rotations.[12,42] The results for atomic species were complemented with entropic corrections applying the Sackur-Tetrode equation assuming an ideal gas and Maxwell-Boltzmann statistics.[43] The RI approximation was used for all PBE, MP2 and CCSD(T) calculations.[44,45] All methods were used together with a triple- ζ set of Gaussian basis functions (def2-TZVPP).[46] The levels of approximation are denoted PBE-D3/TZ, MP2/TZ and CCSD(T)/TZ in the following. Radical species are denoted by the symbol “•” and found to exhibit doublet spin states. All other species involved in this study exhibit a singlet ground state with the exception of P(*t*-C₄H₉) and PH (triplet ground state). Maximum deviation of the ideal values for the $\langle S^2 \rangle$ operator are <0.03 for the radical species indicating single-reference character suitable for the unrestricted Kohn-Sham/Hartree-Fock methods applied. The electronic states have been consistently confirmed by the presented PBE-D3, MP2 and CCSD(T) calculations in line with previous results on GaCH₃, PH and PH₃. [47,48] The accuracy of the methods applied was measured by comparing the energies to high level CCSD(T)/TZ data and will be presented in the results section 3.4. To our knowledge, experimental thermodynamic data are unfortunately not available for the reactions investigated here. In the Supplementary Information, the structures derived are compared to available experimental data.[49-52]

3 Results

A catalogue of 61 elementary decomposition reactions was assembled and electronic reaction energies of these reactions were calculated with PBE-D3/TZ, MP2/TZ and CCSD(T)/TZ. Thermodynamic corrections were added for low pressure atmospheres (0.05 atm) and temperatures of 400 °C, 500 °C and 675 °C according to the experimental growth conditions. In the following sections, we present the data for the reaction energies of (i) decomposition of TEG, (ii) decomposition of TBP and (iii) selected transition state energies for TEG and TBP. In the first two sections, uni- and bimolecular reactions are considered separately. Higher order reactions were not considered here due to the low pressure environment. Furthermore, four different possible classes of decompositions were considered for unimolecular reactions: (a) Homolytical bond cleavage, (b) β -hydrogen elimination, (c) alkane elimination and (d) H₂ elimination. Three classes were considered for bimolecular decompositions: Alkane elimination with a (a) hydrogen radical (H•), (b) alkyl (ethyl, *tert*-butyl) radical (C₂H₅•, *t*-C₄H₉•) or (c) molecular hydrogen (H₂) as reaction partner.

3.1 Thermodynamics of decomposition reactions of TEG

The reaction energies for unimolecular decomposition reactions of TEG are presented in Table 1. Four mechanism classes are listed with elementary reactions of the original precursors and its decomposition products. All of the reactions shown are endoenergetic ($\Delta E > 0$), while β -hydride alkane eliminations are exergonic ($\Delta G < 0$) for elevated temperatures. This is due to entropic effects resulting in large differences between ΔE and ΔG values. Higher temperatures therefore favor these decomposition reactions. The general ordering (from the least to the most favorable reactions considering ΔE) of the investigated decomposition mechanisms is homolytical cleavages \ll β -hydride eliminations $<$ H₂ eliminations $<$ alkane eliminations.

The reaction energies for bimolecular decomposition reactions of TEG are presented in Table 2. Here, all reactions listed are energetically accessible. Entropy effects are much smaller since the number of reactants does not change from educts to products (except BG2, BG5). For some radical species the MP2/TZ results deviate considerably from the CCSD(T)/TZ benchmark values (e.g. BG3, BG4, BG7) – the differences are mostly less on the PBE/TZ level. This is in line with the known difficulty of the MP2 method to describe radical species accurately. The energetic ordering of decompositions with the following partners (from least to most favorable) is alkane eliminations with H₂ (BG15-19) $<$ alkane eliminations with alkyl radical (BG12, BG14) $<$ H₂ eliminations with H• radicals (BG9, BG11) $<$ alkane eliminations with H• radicals (BG1, BG4, BG7, BG8) \ll radical recombinations (with or without elimination products; BG2, BG3, BG5, BG6, BG10, BG13). Reactions AG11-14 (β -hydride eliminations), AG19-20 (H₂ eliminations), AG15, AG17 (alkane eliminations) and

BG15-18 (alkane eliminations with H₂) were chosen for subsequent investigations of reaction barriers under the condition of low H• concentration.

3.2 Thermodynamics of decomposition reactions of TBP

The reaction energies for unimolecular decomposition reactions of TBP are presented in Table 3. Most of the reactions are energetically and thermodynamically unfavorable. Only β-hydrogen eliminations (AP6, AP7) are exothermic, although the entropy effects are very large for all unimolecular reactions. For the P-containing species a good agreement was found between the computational methods applied except for AP9 and AP12 which can be attributed to the difficulty of DFT dealing with atomic species. The reaction energies for bimolecular decomposition reactions of TBP are presented in Table 4. All eliminations are energetically (except BP8) and thermodynamically accessible. As for the bimolecular reactions with Ga species, entropic effects are small (except BP8, which results in three species). Reactions AP6 (β-hydrogen elimination) and BP8 (alkene + H₂ elimination with H₂) were chosen for the subsequent transition state analysis. No transition state could be found for reaction BP7.

To summarize the part of the study focusing on the reaction energies: Unimolecular decomposition reactions exhibit much larger changes in ΔG upon considering increasing temperatures compared to bimolecular reactions. As expected, all reactions leading from radical species to saturated products are exergonic (see also ref. [10]) while larger radical species tend to be more stabilized than small ones. All β-hydrogen eliminations (alkene eliminations) are exergonic (Ga and P species) and so are many uni- and bimolecular alkane and H₂ eliminations from Ga species. All unimolecular H₂ and alkane eliminations from P species are endergonic. This catalogue's bimolecular decompositions are, generally, exergonic. Gas phase reactivity cannot be understood from the thermodynamic data alone. However they give a strong hint which reaction classes are relevant for the investigation of reaction kinetics in terms of transition state theory. This will be described for the reactions indicated in the previous paragraphs in the next section.

3.3 Transition states of TEG and TBP decompositions

Several elementary decompositions were identified from the catalogue presented in Tables 1-4, where the thermodynamic data indicate their importance for the gas phase decomposition chemistry of the MOVPE growth of GaP. For those reactions, transition states linking reactants and products of the reactions in Tables 1-4 were investigated. Subsequently, possible decomposition pathways were formulated which determine the possible decomposition products. Furthermore, those pathways contain the structural data which provides a rationalization of the underlying reaction mechanisms.

The selection criteria for the reactions considered in this section are: (i) elementary steps are exergonic, (ii) they do not depend on any other species than the carrier gas H_2 (which is present in sufficient concentration), and (iii) the reactant species will realistically be available either as original precursor or via exclusively exergonic preceding reactions. The transition states (TS) were optimized with PBE-D3/TZ.

The electronic activation energies of the selected reactions and the frequencies of the transition state modes are given in Table 5. The energies vary from 67.3 (BG18) to 312.3 kJ mol⁻¹ (AG15) exemplifying the strong differences between barriers for different mechanisms. It becomes clear that the barriers for TEG and derived species are much lower compared to the two barriers investigated for decomposition reactions of TBP (except AG15). It is also striking that entropy has a much smaller influence on the barrier height compared to the reaction energies (Tables 1-4), except for the bimolecular reactions involving H_2 (BG15 – BG18, BP8), where the barriers are drastically increased by the inclusion of entropic effects. This can be understood in terms of the entropy-lowering association of two species to one transition structure in the bimolecular case. The vibrational modes of the TS structures connecting educts and products can also be taken to distinguish the different mechanism classes: Transition states containing H_2 exhibit much higher mode energies (> 1100 cm⁻¹) compared to alkane elimination reactions (377 – 717 cm⁻¹). Before discussing the implications of the reaction catalogue introduced, an evaluation of the accuracy for the methods chosen will be presented.

3.4 Accuracy of PBE-D3/TZ and MP2/TZ vs. CCSD(T)/TZ

In order to validate the accuracy of the broadly applicable PBE-D3/TZ and MP2/TZ methods, statistical data regarding the deviations from the highly accurate CCSD(T)/TZ computations are given in Table 6. All presented deviation criteria of PBE-D3/TZ energies are of the same order as the respective deviations of MP2/TZ energies with respect to CCSD(T)/TZ//MP2/TZ. This validation of PBE-D3 is important as for calculations of larger systems the application of DFT-based methods will be preferred over costly post-HF methods, especially for investigations of surface-assisted reactions where the MP2 method is currently only feasible for small systems. Energies of reactions where radical species are involved have a larger deviation and represent the respective maximum absolute deviations of this catalogue's reactions. This is known for species with an unpaired electron and mainly due to the inaccurate exchange contribution to the energy in GGA exchange-correlation functionals.[54] However, focusing on decomposition reaction energies, the description of even large radicals by PBE-D3/TZ seems to be of sufficient accuracy relative to CCSD(T)/TZ.

The relative and absolute deviation of the examined energy barriers is larger, as it is known for GGA to underestimate reaction barriers.[55] Remarkably, RMS, RAD and MAE of

PBE-D3/TZ is smaller than MP2/TZ with respect to CCSD(T)/TZ. This overestimation of activation energies is a known shortcoming of MP2. Similar trends of reaction energy deviations for DFT relative to CCSD(T)/TZ were also found in other studies on Ga precursor decompositions.[12] In conclusion, the accuracy of the methods is sufficient for the purpose of identifying relevant decomposition products and analyzing the respective mechanisms.

In the following, uni- and bimolecular decomposition schemes including mainly exergonic reactions are presented for TEG and TBP. From those schemes several pathways were assembled involving the reaction energies together with the reaction barriers presented above.

3.5 Decomposition scheme for TEG

In the light of the results given in Tables 1 and 2, the plethora of possible reactions is reduced to the following set: Unimolecular β -hydride eliminations or homolytical bond cleavages of the Ga-C, C-C or C-H can be formulated for TEG. Furthermore, recombinative eliminations of alkanes or hydrogen are energetically accessible for some decomposition products. In the bimolecular case, alkane and H₂ eliminations are possible with reactants like H₂ or radicals (H•, C₂H₅•). This leads to the decomposition pathways of first (Figure 1a) and second (Figure 1b) order reactions. However, all homolytical cleavage reactions of saturated species are endoenergetic and endergonic and are not considered further in this study. Specifically, the bond energies for TEG were calculated as 404.6 kJ mol⁻¹ for the terminal C _{β} -H bond, 376.2 kJ mol⁻¹ for the C _{α} -C _{β} bond and 292.3 kJ mol⁻¹ for the Ga-C bond (AG2, AG3, AG1 for PBE-D3/TZ in Table 1). As a consequence, the remaining pathways build a decomposition scheme for TEG. The major pathways are discussed in the following subsections in detail.

Pathway 1, “ β -hydride eliminations”

The possibility of reaction via β -hydride elimination is a significant advantage of TEG compared to, for instance, TMG which has been studied extensively for CVD applications.[12] Since a carbon atom in β -position to gallium is absent in TMG, only endergonic homolytical cleavages can occur, hence a decomposition is less likely.[15] The suggested decomposition pathway 1 for TEG has four elementary steps and leads to GaH as the smallest thermodynamically accessible Ga species (see Figure 2). Firstly, ethylene is eliminated from TEG in a β -hydride elimination step with a Gibbs energy barrier of $\Delta G_{400}^{\#} = 141.0$ kJ mol⁻¹. The transition state is rather symmetric with $d(\text{Ga-H}) = 1.697$ Å and $d(\text{C-H}) = 1.718$ Å. The same is true for the following further β -hydride elimination steps with barriers of $\Delta G_{400}^{\#} = 149.9$ and $\Delta G_{400}^{\#} = 129.2$ kJ mol⁻¹, respectively, leading to GaH₃. A reduction in the Ga-C, Ga-H and H-C bond lengths thereby points to slightly earlier transition states for the less substituted Ga species. And indeed, the trend in electronic barriers ($\Delta E^{\#} = 131.6, 128.1$

and $123.8 \text{ kJ mol}^{-1}$, Table 1) confirms this assumption. Entropy covers this effect and leads to the observed different trend in ΔG^\ddagger . The fourth step within this pathway exhibits the highest barrier. The H_2 elimination from GaH_3 is slightly exergonic and has a barrier of $\Delta G^\ddagger_{400} = 200.5 \text{ kJ mol}^{-1}$. The subsequent homolytical cleavage to $\text{Ga}\cdot$ and $\text{H}\cdot$ is highly endergonic in the gas phase ($\Delta G_{400} = 192.0 \text{ kJ mol}^{-1}$, see Table 1). Hence, via this pathway GaH_3 will likely be the main product with the possibility of GaH at elevated temperatures. From the graphical representation, it appears that the differences in the reaction profile with rising temperature might be due to entropy effects on the transition states. But a closer analysis of the numbers in Tables 1 and 5 reveals that the temperature effects for the intermediates are much stronger compared to the transition states.

Pathway 2, “n-butane elimination”

A recombinative elimination of n-butane from TEG leads to monoethylgallium ($\text{Ga}(\text{C}_2\text{H}_5)$) in a single step (Figure 3), but the barrier for this reaction is very large ($\Delta G^\ddagger_{400} = 326.2 \text{ kJ mol}^{-1}$) and unlikely to be surmounted even under elevated temperatures. If monoethylgallium can be formed by any (e.g. surface-assisted) process, a β -hydride elimination may result in gallium monohydride (GaH) in a low barrier step ($\Delta G^\ddagger_{400} = 82.6 \text{ kJ mol}^{-1}$). GaH is an interesting intermediate as it can be formed from many different sources (see Figure 1).

Pathway 3, “monoethylgallane decomposition processes”

Next to the low-barrier β -hydride elimination described in pathway 1, monoethylgallane can directly decompose to GaH (Figure 4, reaction to the right) by the elimination of ethane ($\Delta G^\ddagger_{400} = 199.8 \text{ kJ mol}^{-1}$). Furthermore, H_2 elimination to $\text{Ga}(\text{C}_2\text{H}_5)$ (Figure 4, reaction to the left) can occur with a higher barrier of $\Delta G^\ddagger_{400} = 215.6 \text{ kJ mol}^{-1}$. Since both processes are thermodynamically and kinetically less favorable than the β -hydride elimination (Figure 2), they are not highly relevant gas phase reactions.

Pathway 4, “2nd order pathway, ethane elimination”

The bimolecular decomposition reactions with a radical reactant or H_2 are exergonic. A highly interlinked decomposition network can be formulated (Fig. 1b) leading to both, radical and non-radical products. Formally, atomic Ga can be reached via an alkane elimination pathway with hydrogen radicals $\text{H}\cdot$ as reactant (e.g. $\Delta G_{400}(\text{BG1}) = -156.6 \text{ kJ mol}^{-1}$, Table 2). Assuming low concentrations of those radicals in the gas phase for thermodynamic reasons (H_2 dissociation: $\Delta G_{400} = 326.4 \text{ kJ mol}^{-1}$) no barrier was calculated for such elimination steps. Reactions with molecular hydrogen (H_2), which is used as carrier gas and available in high concentrations, are more likely. The pathway shown in Figure 6 contains three steps of H_2 addition reactions to saturated Ga species, which decompose under simultaneous ethane elimination in subsequent steps to $\text{Ga}(\text{C}_2\text{H}_5)_2\text{H}$, $\text{Ga}(\text{C}_2\text{H}_5)\text{H}_2$ and GaH_3 , respectively. Note

that electronic barriers are lower throughout compared to the corresponding unimolecular β -hydride elimination barriers of those species (Table 5), although an additional H-H bond is broken. However, upon applying thermodynamic corrections to the transition state energies of this bimolecular decomposition class the barriers are drastically increased. The very high initial barrier for the H_2 -assisted reaction (BG1, $\Delta G_{400}^\# = 208.5 \text{ kJ mol}^{-1}$) indicate that the decomposition reactions via second-order reactions are less important.

Comparing uni- and bimolecular alkyl eliminations from gallane species (Figures 2 and 5) yet another trend can be observed: While the thermodynamics of unimolecular β -hydride eliminations strongly depend on temperature (Fig. 2), this is not the case for the bimolecular C_2H_6 eliminations of the same species (Fig. 5). On the other hand, the barriers are significantly rising with increasing temperature for the bimolecular classes, whereas the unimolecular barriers are not affected by temperature (see also Table 5).

3.6 Decomposition scheme for TBP

Building upon the data presented in Tables 3 and 4, a decomposition scheme for TBP (Figure 6) can be set up similar to TEG (Figure 1). The reaction energies lead to the conclusion that TBP can decompose via homolytical bond cleavages and the elimination of hydrogen gas, alkane or alkene compounds, respectively. As it turns out, most unimolecular reactions (Fig. 6a) can be neglected, since they are strongly endergonic (Table 3). Considering reactions with H_2 , a hydrogen or alkyl radical (e.g. $H\cdot$, $t\text{-}C_4H_9\cdot$), a bimolecular decomposition scheme of exclusively exergonic reactions can be formulated which involves radical and non-radical intermediate species. Within this scheme (Fig. 6b), no P species smaller than the radical $PH_2\cdot$ can be reached from TBP. If dehydrogenated P($t\text{-}C_4H_9$) is present, PH and atomic P can be reached on exergonic paths. The major pathways are discussed in the following.

Pathway 5 “ β -hydrogen elimination”

Fan et al. propose an “intramolecular β -hydrogen elimination” mechanism for TBP, confirmed by temperature-dependent FT-IR measurements performed during MOVPE in a H_2 atmosphere similar to the conditions in our study.[56] This exergonic alkene elimination ($i\text{-}C_4H_8$, isobutene) is the only unimolecular decomposition mechanism considered here as all other classes are highly endergonic. It can be formulated for TBP as well as the triplet species P($t\text{-}C_4H_9$) (AP6, AP7). It involves the transfer of a hydrogen atom from a β -carbon atom of the butyl group to the phosphorous center. As the formal acceptor orbital of the P atom is occupied, the reaction cannot directly be compared to the β -hydride mechanism discussed for the Ga species (which exhibits an empty p-orbital).[57] A transition state with a rather large P-C distance was found (left path in Figure 7). A detailed analysis of this reaction class is beyond the scope of this study and will be presented elsewhere.[58] The barrier for

this reaction (AP6, $\Delta G_{400}^{\#} = 217.4 \text{ kJ mol}^{-1}$) is significantly higher than typical barriers of the calculated β -hydride eliminations of Ga species (AG11 – AG14, $\Delta G_{400}^{\#} = 82.6 - 149.9 \text{ kJ mol}^{-1}$). Furthermore, the trend of Gibbs energy barriers for the reaction with increasing temperature is reversed with respect to the Ga β -hydride eliminations indicating differences in the mechanism. The equivalent decomposition from the triplet $P(t\text{-C}_4\text{H}_9)$ will not be discussed in detail here since its formation from TBP by eliminating H_2 is endergonic (AP10, $\Delta G_{400} = 123.2 \text{ kJ mol}^{-1}$).

Pathway 6 “second order pathway, alkane elimination”

The bimolecular decomposition network of TBP is less interlinked compared to the bimolecular network of Ga species, since only a small number of decomposition products can be formulated. Reactions of TBP with a radical may lead to $P(t\text{-C}_4\text{H}_9)\text{H}\cdot$ or $\text{PH}_2\cdot$, from which recombination with further radical partners (e.g. $\text{H}\cdot$) may lead to the original precursor or phosphine (PH_3). The most important bimolecular decomposition pathway for TBP is the exergonic concerted elimination of isobutene and H_2 . A transition state can be found for this single-step reaction and is very high in energy (BP8, $\Delta E^{\#} = 264.6 \text{ kJ mol}^{-1}$). As expected for a bimolecular reaction, the unfavorable entropy factor increases this barrier even further to $\Delta G_{400}^{\#} = 337.3 \text{ kJ mol}^{-1}$ rendering it highly improbable that this barrier could be overcome at the given temperature (see right path in Figure 7). Several bimolecular reactions can be formulated for $P(t\text{-C}_4\text{H}_9)$, but applying the assumption given above (low reactant concentration due to missing decomposition pathways of TBP to this intermediate) no reaction barrier was calculated for those. Considering the thermodynamic schemes of both uni- and bimolecular decomposition pathways from TBP, only phosphine (PH_3) is likely to be formed in significant concentrations aside the original precursor in the gas phase. Notably, it is known from experiment that the fraction of original precursor finally arriving on the surface is very large for P species[4,56] in line with the large barriers presented here.

4 Discussion

The results presented in the previous sections will be discussed in the light of the assumptions presented earlier. In the first results section, thermodynamic data was presented for many elementary reactions starting from the precursors TEG ($\text{Ga}(\text{C}_2\text{H}_5)_3$) and TBP ($\text{PH}_2(t\text{-C}_4\text{H}_9)$). Of course, it cannot be excluded that a reaction might be missing in the catalogue but considering the large amount of data and the various mechanism classes we are confident to have included the important reactions. Initially, all fragments were further investigated even when no direct route to this fragment was found. This enables a complete picture of the Ga and P species and a comprehensive evaluation of the methodology. The reaction channels described here encompass uni- and bimolecular reactions. As pointed out in the introduction, unimolecular reactions are assumed to occur more likely than higher order reactions in a low-pressure atmosphere. Calculations of homolytical bond cleavages (e.g. symmetric dissociation of H_2 , cleavages of $\text{H}\cdot$, $\text{CH}_3\cdot$, and $\text{C}_2\text{H}_5\cdot$ from TEG) show that this decomposition class is consistently endergonic (for saturated reactants) and can therefore be neglected. Instead, β -hydride elimination reactions seem to be the dominant channel for TEG.

Additionally, some classes of bimolecular reactions have to be considered. These are reactions with the carrier gas H_2 which are thermodynamically accessible. But also the radicals $\text{H}\cdot$, $\text{C}_2\text{H}_5\cdot$, $t\text{C}_4\text{H}_9\cdot$, etc. might be available in small concentrations as they can be produced in the course of a MOVPE procedure. Especially interesting is the formation of atomic hydrogen which can potentially be thermally desorbed from the substrate at 480 - 580 °C [16] as well as hydrogen (or carbon hydrates) via recombinative desorption.[59] As this work focused on pure gas phase reactions, the investigation of the latter reactions only becomes important when the surface is explicitly considered in the next phase of this study. Heterolytic dissociation reactions leading to ionic species are not considered as those will not occur in the gas phase and are of minor importance when focusing on relevant decomposition products. For example, an alternative (“barrierless”) mechanism for reaction AP6 involving an unstable, ionized intermediate step was proposed for the As-precursor TBA,[15] but the mechanism is probably surface-mediated. It becomes clear that the conclusions about viability of a reaction mechanism cannot be drawn from the thermodynamic data alone. Reaction barriers were calculated only for those exergonic reactions that were likely to occur based on the above assumptions. AP6, for instance, is strongly exergonic but exhibits a large barrier which will result in a very low reaction rate at all but the highest temperatures. Generally, transition state theory is valid here as large molecules and high temperatures are considered.[48]

The distribution of particles and temperature in the chamber is irregularly fluctuating. The Si-wafer is locally heated, so the highest temperature region is at and directly above the

surface. The carrier gas flow induces a flux that transports heated gas away from the wafer towards the gas outlet. As a consequence, the temperatures applied in this study (experimental surface temperatures of 400, 500 and 675 °C) represent upper bounds for the temperature in the gas phase. This has consequences interpreting the calculated energies: Since the change in Gibbs energy becomes more negative (or less positive) with increasing temperature for all elementary reactions, a higher temperature means a more exergonic reaction. Thus, the presented thermodynamic values represent a lower bound for the discussed MOVPE precursors. In the real system, the reaction enthalpies will be less favorable due to colder local temperatures further away from the surface. The situation is different for the reaction barriers: As the barrier of a reaction generally *increases* with increasing temperature (except AG20, AP6), the calculated data are upper bounds for the barriers. In the real system, lower temperatures will result in smaller barriers. However, as the temperature dependence of Gibbs energy barriers is not strong, this effect will not be decisive. More important will be the higher kinetic energy of the molecules to overcome these (slightly raised) barriers at higher T.

Decompositions on the surface have entirely different mechanisms and may lead to different inert and reactive intermediates. Catalytic effects of the surface might change the relevant barriers drastically, hence studies on this field have to be taken into account.[16,60] Thus we will continue our work in this field by applying periodic calculations to the GaP/Si system within the methodology validated here.

5 Conclusions

In this study, we present a comprehensive reaction catalogue for the gas phase decomposition reactions of triethylgallane ($\text{Ga}(\text{C}_2\text{H}_5)_3$, TEG) and tertiarybutylphosphine ($\text{PH}_2(t\text{-C}_4\text{H}_9)$, TBP) with thermodynamic and reaction barrier data based on DFT and ab initio (MP2, CCSD(T)) energies. From these data, conclusions can be drawn for the gas phase species relevant for the MOVPE growth of III/V-semiconductor GaP on silicon substrates. For TEG, we find a series of β -hydride elimination reactions as the most probable pathway leading to GaH_3 or even GaH at elevated temperatures (675 °C). Radical cleavage and other reactions as often proposed earlier are found to exhibit unfavorable thermodynamic characteristics. For TBP, a group 15 analogue of the β -hydride elimination reaction is found as the energetically most accessible reaction. For all uni- and bimolecular TBP decomposition reactions, the computed barriers are very high leading to the conclusion of mainly the original precursor arriving at the surface. Methodologically, we could show that dispersion-corrected DFT computations at the PBE-D3 level performs well in comparison to MP2 and CCSD(T) benchmark data and can be used for further studies of these systems.

6 Acknowledgements

We thank Prof. Kerstin Volz, Prof. Wolfgang Stolz and Dr. Andreas Beyer (Marburg) for fruitful discussions and insight into experimental details. Funding by the DFG through the Research Training Group “Functionalization of Semiconductors” (GRK 1782) is gratefully acknowledged. A.S. thanks the Beilstein Institut, Frankfurt am Main for generous support via a PhD fellowship. Computational resources were kindly provided by HRZ Marburg, LOEWE-CSC Frankfurt and HLR Stuttgart.

7 References

- [1] a) B. Kunert, K. Volz, I. Németh, W. Stolz, *J. Lumin.*, **2006**, *121*, 361. b) N. Koukourakis, C. Buckers, D. A. Funke, N. C. Gerhardt, S. Liebich, S. Chatterjee, C. Lange, M. Zimprich, K. Volz, W. Stolz, B. Kunert, S. W. Koch, M. R. Hofmann, *Appl. Phys. Lett.* **2012**, *100*, 092107; c) B. Kunert, K. Volz, J. Koch, W. Stolz, *Appl. Phys. Lett.* **2006**, *88*, 182108; d) S. Liebich, M. Zimprich, A. Beyer, C. Lange, D. J. Franzbach, S. Chatterjee, N. Hossain, S. J. Sweeney, K. Volz, B. Kunert, W. Stolz, *Appl. Phys. Lett.* **2011**, *99*, 071109; e) B. Kunert, K. Volz, W. Stolz, *Phys. Status Solidi B*, **2007**, *244*, 2730.
- [2] D. Liang, J. E. Bowers, *Nat. Photonics* **2010**, *4*, 511.
- [3] B. Kunert, K. Volz, J. Koch, W. Stolz, *J. Cryst. Growth*, **2007**, *298*, 121.
- [4] A. Beyer, J. Ohlmann, S. Liebich, H. Heim, G. Witte, W. Stolz, K. Volz, *J. Appl. Phys.*, **2012**, *111*, 83534.
- [5] A. Beyer, I. Németh, S. Liebich, J. Ohlmann, W. Stolz, K. Volz, *J. Appl. Phys.*, **2011**, *109*, 083529.
- [6] P. Gibart, *Rep. Prog. Phys.*, **2004**, *67*, 667.
- [7] C. Wang, *J. Cryst. Growth*, **2004**, *272*, 664.
- [8] M. Jacko, S. J. W. Price, *Can. J. Chem.*, **1963**, *41*, 1560.
- [9] A. Brauers, *Prog. Cryst. Growth Charact. Mater.*, **1991**, *22*, 1.
- [10] M. Trachtman, S. Beebe, *J. Phys. Chem.*, **1995**, 15028.
- [11] D. Moscatelli, P. Caccioppoli, C. Cavallotti, *Appl. Phys. Lett.*, **2005**, *86*, 91106.
- [12] R. Schmid, D. Basting, *J. Phys. Chem. A*, **2005**, *109*, 2623.
- [13] J. Lee, Y. Kim, T. Anderson, *ECS Trans.* **2009**, *25*, 41.
- [14] T. R. Gow and R. Lin, *J. Cryst. Growth*, **1990**, *106*, 577.
- [15] M. Boero, Y. Morikawa, K. Terakura, M. Ozeki, *J. Chem. Phys.*, **2000**, *112*, 9549.
- [16] N. Bahlawane, F. Reilmann, L.-C. Salameh, K. Kohse-Höinghaus, *J. Am. Soc. Mass*

- Spec.*, **2008**, *19*, 947.
- [17] A. Saxler, D. Walker, P. Kung, X. Zhang, M. Razeghi, J. Solomon, W. C. Mitchel, H. R. Vydyanath, *Appl. Phys. Lett.*, **1997**, *71*, 3272.
- [18] B. Wolbank, R. Schmid, *Chem. Vap. Deposition*, **2003**, *9*, 272.
- [19] a) S. H. Li, C. A. Larsen, N. I. Buchan, G. B. Stringfellow, *J. Electron. Mater.* **1989**, *18*, 457; b) Y. S. Hiraoka, M. Mashita, T. Tada, R. Yoshimura, *Appl. Surf. Sci.* **1992**, *60-1*, 246; c) C. H. Chen, D. S. Cao, G. B. Stringfellow, *J. Electron. Mater.* **1988**, *17*, 67;
- [20] K. Volz, A. Beyer, W. Witte, J. Ohlmann, I. Németh, B. Kunert, W. Stolz, *J. Cryst. Growth*, **2011**, *315*, 37.
- [21] A. Y. Timoshkin, *Coord. Chem. Rev.*, **2005**, *249*, 2094.
- [22] A. Y. Timoshkin, H. F. Schaefer III, *J. Phys. Chem. C*, **2008**, *112*, 13816.
- [23] A. Y. Timoshkin, H. F. Bettinger, H. F. Schaefer III, *J. Cryst. Growth*, **2001**, *222*, 170.
- [24] B. Mondal, D. Mandal, D. Ghosh, A. K. Das, *Journal Phys. Chem. A*, **2010**, *114*, 5016.
- [25] J. Schäfer, A. Simons, J. Wolfrum, R. A. Fischer, *Chem. Phys. Lett.*, **2000**, *319*, 477.
- [26] A. Szabó, A. Kovács, G. Frenking, *Z. Anorg. Allg. Chem.*, **2005**, *631*, 1803.
- [27] A. Y. Timoshkin, G. Frenking, *J. Am. Chem. Soc.*, **2002**, *124*, 7240.
- [28] G. Zimmermann, A. Ougazzaden, A. Gloukhian, *Mater. Sci. Eng.*, **1997**, *B44*, 37.
- [29] S. J. Hashemifar, P. Kratzer, M. Scheffler, *Phys. Rev. B*, **2010**, *82*, 214417.
- [30] Frisch, M. J.; Trucks, G. W.; Schlegel, H. B.; Scuseria, G. E.; Robb, M. A.; Cheeseman, J. R.; Scalmani, G.; Barone, V.; Mennucci, B.; Petersson, G. A.; Nakatsuji, H.; Caricato, M.; Li, X.; Hratchian, H. P.; Izmaylov, A. F.; Bloino, J.; Zheng, G.; Sonnenberg, J. L. H., M.; Ehara, M.; Toyota, K.; Fukuda, R.; Hasegawa, J.; Ishida, M.; Nakajima, T.; Honda, Y.; Kitao, O.; Nakai, H.; Vreven, T.; Montgomery, Jr., J. A.; Peralta, J. E.; Ogliaro, F.; Bearpark, M.; Heyd, J. J.; Brothers, E.; Kudin, K. N.; Staroverov, V. N.; Kobayashi, R.; Normand, J.; Raghavachari, K.; Rendell, A.; Burant, J. C.; Iyengar, S. S.; Tomasi, J.; Cossi, M.; Rega, N.; Millam, N. J.; Klene, M.; Knox, J. E.; Cross, J. B.; Bakken, V.; Adamo, C.; Jaramillo, J.; Gomperts, R.; Stratmann, R. E.; Yazyev, O.; Austin, A. J.; Cammi, R.; Pomelli, C.; Ochterski, J. W.; Martin, R. L.; Morokuma, K.; Zakrzewski, V. G.; Voth, G. A.; Salvador, P.; Dannenberg, J. J.; Dapprich, S.; Daniels, A. D.; Farkas, Ö.; Foresman, J. B.; Ortiz, J. V.; Cioslowski, J.; Fox, D. J. ; Gaussian 09, Rev. C.01, Gaussian, Inc.: Wallingford CT, 2009.
- [31] TURBOMOLE V6.3, a development of University of Karlsruhe and Forschungszentrum Karlsruhe GmbH, 1989-2007, TURBOMOLE GmbH, since 2007; available from www.turbomole.com, **2012**.
- [32] R. Ahlrichs, M. Bär, M. Häser, H. Horn, C. Kölmel, *Chem. Phys. Lett.*, **1989**, *162*, 165.
- [33] J. P. Perdew, K. Burke, M. Ernzerhof, *Phys. Rev. Lett.*, **1996**, *77*, 3865.
- [34] S. Grimme, J. Antony, S. Ehrlich, H. Krieg, *J. Chem. Phys.*, **2010**, *132*, 154104.

- [35] S. Grimme, S. Ehrlich, L. Goerigk, *J. Comput. Chem.*, **2011**, *32*, 1456.
- [36] O. Christiansen, H. Koch, P. Jørgensen, *Chem. Phys. Lett.*, **1995**, *243*, 409.
- [37] C. Hättig, F. Weigend, *J. Chem. Phys.*, **2000**, *113*, 5154.
- [38] F. Weigend, M. Häser, H. Patzelt, R. Ahlrichs, *Chem. Phys. Lett.*, **1998**, *294*, 143.
- [39] C. Hättig, A. Hellweg, A. Köhn, *Phys. Chem. Chem. Phys.*, **2006**, *8*, 1159.
- [40] P. Deglmann, F. Furche, *J. Chem. Phys.*, **2002**, *117*, 9535.
- [41] P. Deglmann, F. Furche, R. Ahlrichs, *Chem. Phys. Lett.*, **2002**, *362*, 511.
- [42] M. Tafipolsky, R. Schmid, *J. Comput. Chem.*, **2005**, *26*, 1579.
- [43] O. Sackur, *Ann. Phys.*, **1911**, *36*, 958.
- [44] K. Eichkorn, O. Treutler, H. Ohm, M. Häser, R. Ahlrichs, *Chem. Phys. Lett.* **1995**, *242*, 652.
- [45] F. Weigend, *Phys. Chem. Chem. Phys.* **2006**, *8*, 1057.
- [46] F. Weigend, R. Ahlrichs, *Phys. Chem. Chem. Phys.*, **2005**, *7*, 3297.
- [47] B. C. Hoffman, C. D. Sherrill, H. F. Schaefer III, *J. Mol. Struct. (Theochem)*, **1996**, *370*, 93.
- [48] H. Simka, B. G. Willis, I. Lengyel, *Prog. Cryst. Growth Charact. Mater.*, **1997**, *35*, 117.
- [49] N. W. Mitzel, C. Lustig, R. J. F. Berger, N. Runeberg, *Angew. Chem. Int. Ed. Engl.*, **2002**, *41*, 2519.
- [50] J. R. Durig, *J. Mol. Struct.*, **1977**, *30*, 77.
- [51] a) H. Oberhammer, R. Schmutzler, O. Stelzer, *Inorg. Chem.*, **1978**, *17*, 1254; b) J. Bruckmann, C. Krüger, *Acta Cryst. C*, **1995**, *51*, 1152.
- [52] L. Bartell, H. Burgi, *J. Am. Chem. Soc.*, **1972**, *531*, 5239.
- [53] Test calculations with different partial pressures for the carrier gas H₂ ($5 \cdot 10^{-2}$ atm) and the precursor molecules ($5 \cdot 10^{-4}$ atm) (for an application of this approach see E. Kalered, H. Pedersen, E. Janzén, L. Ojamäe, *Theor. Chem. Acc.* **2013**, *132*, 1) resulted in a constant shift of all reactions containing H₂ as a reactant or product. None of the conclusions regarding endo- or exothermicity of the reactions is affected by this shift.
- [54] D. R. B. Brittain, C. Y. Lin, A. T. B. Gilbert, E. I. Izgorodina, P. M. W. Gill, M. L. Coote, *Phys. Chem. Chem. Phys.*, **2009**, *11*, 1138.
- [55] W. Koch, M. C. Holthausen, *A Chemist's Guide to Density Functional Theory*, Second Edition, Wiley-VCH, Weinheim; New York **2001**.
- [56] G. H. Fan, R. D. Hoare, M. E. Pemble, I. M. Povey, A. G. Taylor, J. O. Williams, *J. Cryst. Growth*, **1992**, *124*, 49.
- [57] a) D. S. Matteson, Chapter 5 in *Organometallic Reaction Mechanisms*, Academic Press, New York and London, **1974** b) J. E. Huheey, E. A. Keiter, R. L. Keiter, *Inorganic Chemistry, Principles of Structure and Reactivity*, 4th Ed., Harber Collins College Publishers, **1993**, p. 699.

[58] A. Stegmüller, R. Tonner, in preparation.

[59] C. Schwalb, M. Dürr, U. Höfer, *Phys. Rev. B*, **2009**, *80*, 085317.

[60] S. Salim, C. K. Lim, K. F. Jensen, *Chem. Mater.*, **1995**, *7*, 507.

Figure captions

Figure 1: Unimolecular (a) and bimolecular (b) decomposition reaction scheme for TEG considering information from Tables 1 and 2. Endergonic steps (at 400 °C) are crossed out or do not appear at all. Decomposition mechanisms are classified as radical cleavages (magenta), alkane (orange), H₂ (yellow) and β-hydride (green) eliminations. Bimolecular eliminations of alkanes or H₂ are considered with the H• (red) or C₂H₅• (turquoise) radicals or H₂ (blue) as reaction partners.

Figure 2. Three-step β-hydride elimination from TEG to gallane (GaH₃), followed by a H₂ elimination step to GaH. Changes in Gibbs energy (ΔG) and barriers relative to the respective reactant (in kJ mol⁻¹) at experimental temperatures. Distances are given in Å.

Figure 3. Two-step decomposition of TEG to GaH via Ga(C₂H₅). Changes in Gibbs energy (ΔG) and barriers relative to the respective reactant (in kJ mol⁻¹) at experimental temperatures. Distances are given in Å.

Figure 4. Monoethylgallane (middle) decomposition to Ga(C₂H₅) (left path) and GaH (right path). Changes in Gibbs energy (ΔG) and barriers (in kJ mol⁻¹) at experimental temperatures. Distances are given in Å.

Figure 6. Bimolecular C₂H₆ eliminations of Ga(C₂H₅)_nH_(3-n) (n = 3,2,1) with reaction partner H₂. Changes in Gibbs energy (ΔG) and barriers relative to the respective reactant (in kJ mol⁻¹) at experimental temperatures. Distances are given in Å.

Figure 6: Unimolecular (a) and bimolecular (b) decomposition reaction scheme for TBP considering information from Tables 3 and 4. Endergonic steps (at 400 °C) are crossed out or do not appear at all. Decomposition mechanisms are classified as radical cleavages (magenta), alkane (orange), H₂ (yellow) and β-hydride (green) eliminations. Bimolecular eliminations of alkanes and/or H₂ are considered with the H• (red) or *t*-C₄H₉• (turquoise) radicals or H₂ (blue) as reaction partners.

Figure 7. Decomposition of TBP via β-hydrogen elimination of isobutene (reaction to the left) and bimolecular concerted elimination of isobutene and H₂ (reaction to the right) leading to phosphine, respectively. Changes in Gibbs energy (ΔG) and barriers (in kJ mol⁻¹) at experimental temperatures. Distances are given in Å.

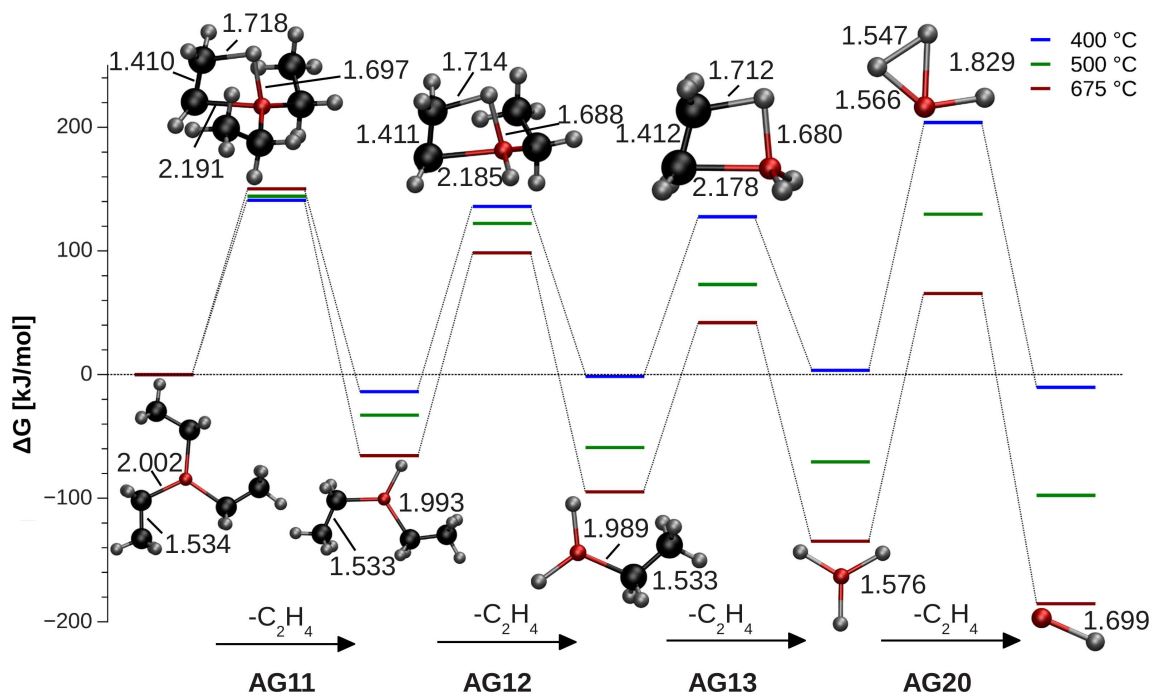


Figure 2

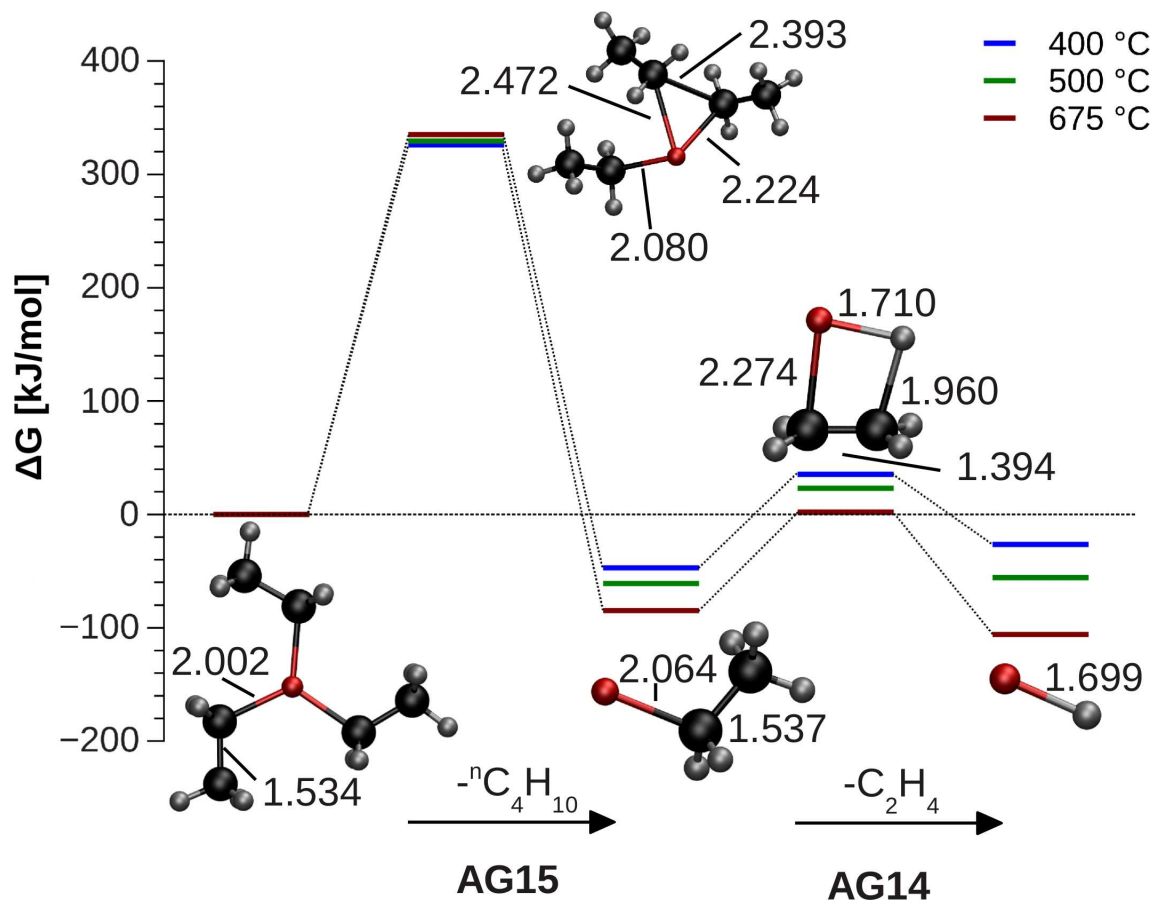


Figure 3

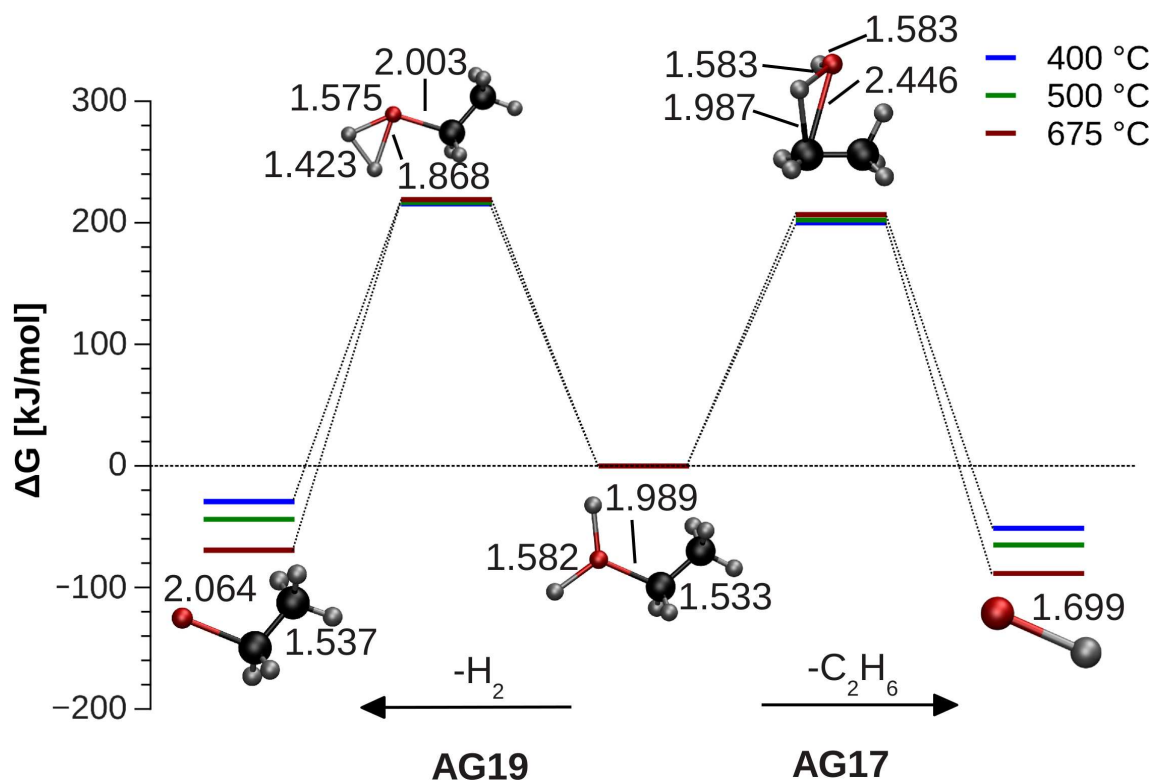


Figure 4

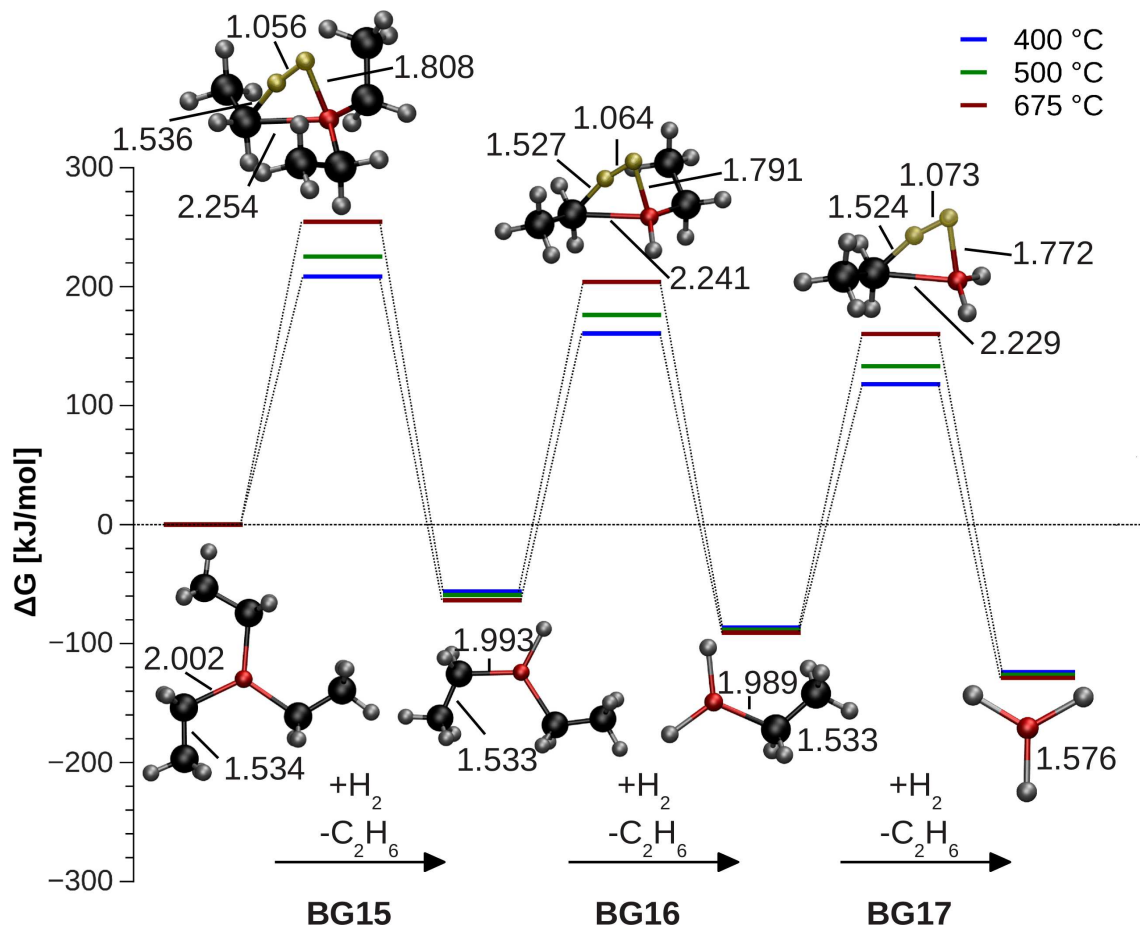


Figure 5

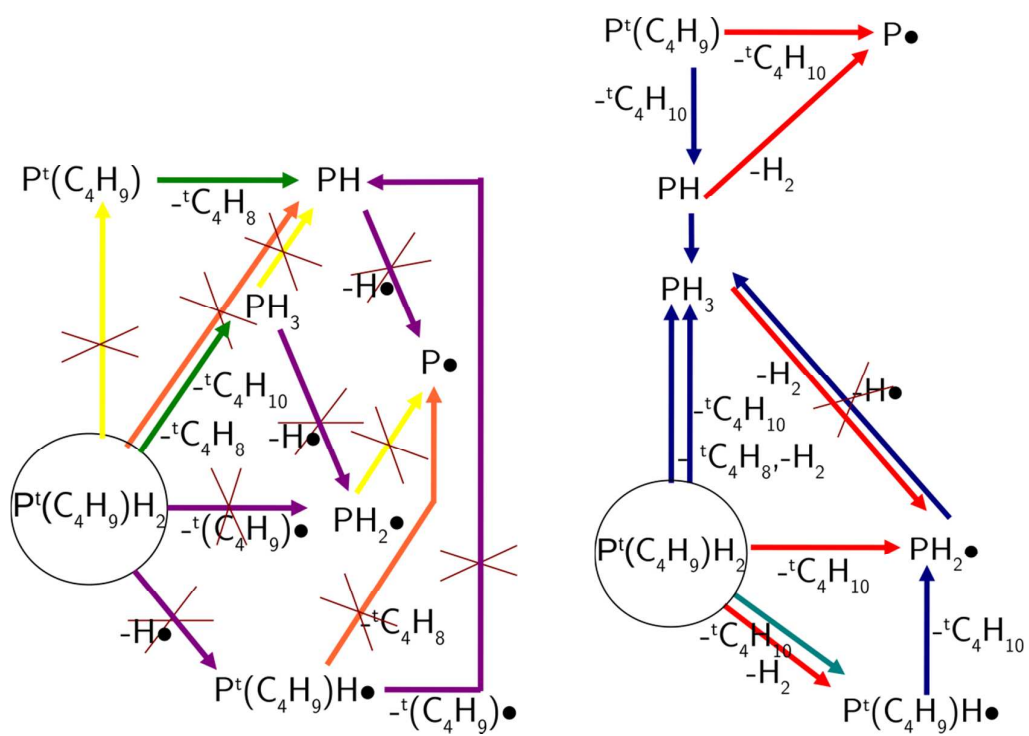


Figure 6

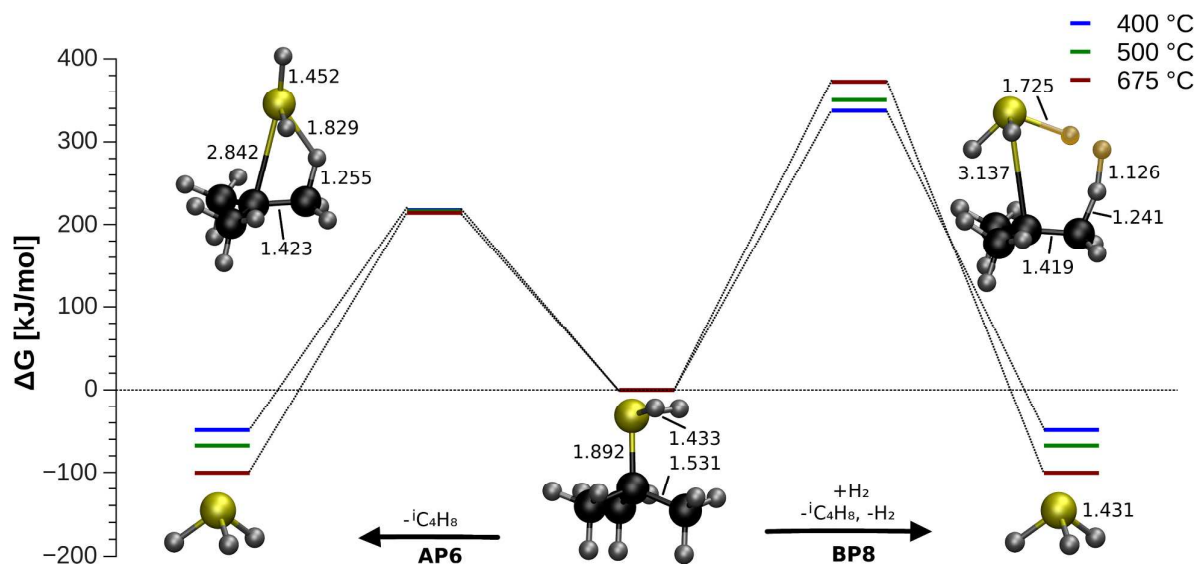


Figure 7

Table 1. Unimolecular decomposition reactions of TEG and related products. Changes in electronic (ΔE) and Gibbs energy (ΔG) for temperatures of 400 °C (a), 500 °C (b) and 675 °C (c) are given in kJ mol^{-1} . Mechanisms are grouped as homolytical bond cleavages (AG1 - AG10), β -hydrogen eliminations (AG11 - AG14), alkane eliminations (AG15 - AG17) and H_2 eliminations (AG18 - AG20).

Reaction index	Reaction scheme	PBE-D3/TZ				MP2/TZ				CCSD(T)/TZ
		ΔE	ΔG a)	ΔG b)	ΔG c)	ΔE	ΔG a)	ΔG b)	ΔG c)	ΔE
AG1	$\text{Ga}(\text{C}_2\text{H}_5)_3 \rightarrow (\text{C}_2\text{H}_5)_2\text{Ga}\cdot + \text{C}_2\text{H}_5\cdot$	292.3	144.3	124.6	90.4	329.4	192.8	174.6	143.2	313.1
AG2	$\text{Ga}(\text{C}_2\text{H}_5)_3 \rightarrow (\text{C}_2\text{H}_5)_2\text{GaC}_2\text{H}_4\cdot + \text{H}\cdot$	404.6	270.8	253.9	224.2	417.4	303.6	289.8	265.4	415.4
AG3	$\text{Ga}(\text{C}_2\text{H}_5)_3 \rightarrow (\text{C}_2\text{H}_5)_2\text{GaCH}_2\cdot + \text{CH}_3\cdot$	376.2	218.6	198.2	162.6	386.2	246.0	228.2	197.2	365.7
AG4	$(\text{C}_2\text{H}_5)_2\text{GaC}_2\text{H}_4\cdot \rightarrow (\text{C}_2\text{H}_5)\text{GaC}_2\text{H}_4 + \text{C}_2\text{H}_5\cdot$	201.4	99.4	82.5	53.2	243.9	108.7	89.7	58.2	245.6
AG5	$(\text{C}_2\text{H}_5)_2\text{Ga}\cdot \rightarrow \text{Ga}(\text{C}_2\text{H}_5) + \text{C}_2\text{H}_5\cdot$	144.8	15.3	-1.8	-31.1	167.5	44.5	28.4	0.6	145.1
AG6	$(\text{C}_2\text{H}_5)_2\text{Ga}\cdot \rightarrow (\text{C}_2\text{H}_5)\text{GaC}_2\text{H}_4 + \text{H}\cdot$	313.6	225.9	211.8	187.0	331.8	218.8	204.9	180.4	347.9
AG7	$(\text{C}_2\text{H}_5)\text{GaC}_2\text{H}_4 \rightarrow \text{GaC}_2\text{H}_4\cdot + \text{C}_2\text{H}_5\cdot$	231.2	62.5	43.8	11.4	250.6	118.5	101.1	70.9	210.0
AG8	$\text{Ga}(\text{C}_2\text{H}_5) \rightarrow \text{GaC}_2\text{H}_4\cdot + \text{H}\cdot$	400.1	273.1	257.3	229.5	414.9	292.8	277.6	250.7	412.8
AG9	$\text{GaH}_3 \rightarrow \text{GaH}_2\cdot + \text{H}\cdot$	337.8	226.9	212.3	186.6	346.8	235.0	220.3	194.5	356.7
AG10	$\text{GaH} \rightarrow \text{Ga}\cdot + \text{H}\cdot$	280.4	192.0	179.0	156.0	273.3	183.6	170.6	147.4	288.0
AG11	$\text{Ga}(\text{C}_2\text{H}_5)_3 \rightarrow \text{Ga}(\text{C}_2\text{H}_5)_2\text{H} + \text{C}_2\text{H}_4$	132.9	-13.8	-32.8	-65.6	141.7	13.8	-2.3	-30.2	127.8
AG12	$\text{Ga}(\text{C}_2\text{H}_5)_2\text{H} \rightarrow \text{Ga}(\text{C}_2\text{H}_5)\text{H}_2 + \text{C}_2\text{H}_4$	133.7	12.3	-2.9	-29.1	140.4	11.9	-4.3	-32.3	126.8
AG13	$\text{Ga}(\text{C}_2\text{H}_5)\text{H}_2 \rightarrow \text{GaH}_3 + \text{C}_2\text{H}_4$	134.8	4.9	-11.6	-40.1	139.3	8.1	-8.5	-37.2	125.9
AG14	$\text{Ga}(\text{C}_2\text{H}_5) \rightarrow \text{GaH} + \text{C}_2\text{H}_4$	140.6	20.6	5.4	-21.1	146.6	24.2	8.7	-18.2	130.4
AG15	$\text{Ga}(\text{C}_2\text{H}_5)_3 \rightarrow \text{Ga}(\text{C}_2\text{H}_5) + n\text{-C}_4\text{H}_{10}$	54.5	-47.1	-61.0	-84.8	86.3	-0.6	-12.4	-32.4	68.5
AG16	$(\text{C}_2\text{H}_5)_2\text{Ga}\cdot \rightarrow \text{GaC}_2\text{H}_4\cdot + \text{C}_2\text{H}_6$	104.4	-12.6	-28.1	-54.8	132.9	26.8	12.6	-11.8	106.7
AG17	$\text{Ga}(\text{C}_2\text{H}_5)\text{H}_2 \rightarrow \text{HGa} + \text{C}_2\text{H}_6$	41.5	-51.3	-65.0	-88.5	67.7	-25.8	-39.6	-63.4	55.3
AG18	$\text{Ga}(\text{C}_2\text{H}_5)_2\text{H} \rightarrow (\text{C}_2\text{H}_5)\text{GaC}_2\text{H}_4 + \text{H}_2$	205.1	125.6	111.8	87.9	242.1	127.3	112.1	85.7	247.4
AG19	$\text{Ga}(\text{C}_2\text{H}_5)\text{H}_2 \rightarrow \text{Ga}(\text{C}_2\text{H}_5) + \text{H}_2$	73.4	-29.4	-44.0	-69.4	93.2	-10.1	-24.7	-50.1	85.4
AG20	$\text{GaH}_3 \rightarrow \text{HGa} + \text{H}_2$	79.3	-13.7	-27.1	-50.4	100.6	6.0	-7.5	-31.2	94.8

Table 2. Bimolecular decomposition reactions of TEG and related products. Changes in electronic (ΔE) and Gibbs energy (ΔG) for temperatures of 400 °C (a), 500 °C (b) and 675 °C (c) are given in kJ mol^{-1} . Mechanisms are grouped as alkane or H_2 eliminations with $\text{H}\cdot$ (BG1 - BG11), $\text{C}_2\text{H}_5\cdot$ (BG12 - BG14) or H_2 (BG15 - BG19) as reaction partner.

Reaction index	Reaction scheme	PBE-D3/TZ				MP2/TZ				CCSD(T)/TZ
		ΔE	ΔG a)	ΔG b)	ΔG c)	ΔE	ΔG a)	ΔG b)	ΔG c)	ΔE
BG1	$\text{Ga}(\text{C}_2\text{H}_5)_3 + \text{H}\cdot \rightarrow (\text{C}_2\text{H}_5)_2\text{Ga}\cdot + \text{C}_2\text{H}_6$	-148.2	-156.6	-159.1	-162.7	-120.2	-117.7	-118.8	-120.0	-138.1
BG2	$(\text{C}_2\text{H}_5)_2\text{Ga}\cdot + \text{H}\cdot \rightarrow \text{Ga}(\text{C}_2\text{H}_5)_2\text{H}$	-330.2	-226.0	-212.1	-187.8	-343.6	-227.9	-212.3	-185.1	-352.9
BG3	$(\text{C}_2\text{H}_5)_2\text{Ga}\cdot + \text{H}\cdot \rightarrow \text{Ga}(\text{C}_2\text{H}_5) + \text{C}_2\text{H}_6$	-295.6	-285.6	-285.4	-284.3	-282.0	-266.0	-265.0	-262.5	-306.1
BG4	$\text{Ga}(\text{C}_2\text{H}_5)_2\text{H} + \text{H}\cdot \rightarrow \text{Ga}(\text{C}_2\text{H}_5)\text{H}\cdot + \text{C}_2\text{H}_6$	-144.2	-132.2	-131.5	-129.5	-120.0	-111.5	-111.6	-111.0	-137.6
BG5	$\text{Ga}(\text{C}_2\text{H}_5)\text{H}\cdot + \text{H}\cdot \rightarrow \text{Ga}(\text{C}_2\text{H}_5)\text{H}_2$	-333.4	-224.4	-209.9	-184.5	-345.0	-235.9	-221.5	-196.2	-354.4
BG6	$\text{Ga}(\text{C}_2\text{H}_5)\text{H}\cdot + \text{H}\cdot \rightarrow \text{GaH} + \text{C}_2\text{H}_6$	-291.9	-275.7	-274.9	-273.0	-277.2	-261.7	-261.1	-259.5	-299.1
BG7	$\text{Ga}(\text{C}_2\text{H}_5)_2\text{H}_2 + \text{H}\cdot \rightarrow \text{GaH}_2\cdot + \text{C}_2\text{H}_6$	-138.7	-137.0	-137.7	-138.3	-119.4	-116.2	-116.9	-117.6	-136.3
BG8	$\text{Ga}(\text{C}_2\text{H}_5) + \text{H}\cdot \rightarrow \text{Ga}\cdot + \text{C}_2\text{H}_6$	-190.3	-156.3	-154.1	-149.9	-185.5	-151.4	-149.5	-145.6	-200.4
BG9	$\text{GaH}_3 + \text{H}\cdot \rightarrow \text{GaH}_2\cdot + \text{H}_2$	-101.0	-99.4	-99.8	-100.2	-86.5	-84.4	-84.8	-85.3	-96.8
BG10	$\text{GaH}_2\cdot + \text{H}\cdot \rightarrow \text{GaH} + \text{H}_2$	-258.5	-240.6	-239.4	-237.1	-246.2	-229.0	-227.8	-225.6	-261.8
BG11	$\text{GaH} + \text{H}\cdot \rightarrow \text{Ga}\cdot + \text{H}_2$	-158.4	-134.4	-133.1	-130.8	-159.9	-135.8	-134.6	-132.4	-165.4
BG12	$\text{Ga}(\text{C}_2\text{H}_5)_3 + \text{C}_2\text{H}_5\cdot \rightarrow \text{Ga}(\text{C}_2\text{H}_5)_2\cdot + n\text{-C}_4\text{H}_{10}$	-90.3	-62.4	-59.3	-53.7	-81.3	-45.1	-40.8	-33.1	-76.5
BG13	$(\text{C}_2\text{H}_5)_2\text{Ga}\cdot + \text{C}_2\text{H}_5\cdot \rightarrow (\text{C}_2\text{H}_5)\text{GaC}_2\text{H}_4 + \text{C}_2\text{H}_6$	-126.8	-75.0	-71.9	-66.2	-117.7	-91.6	-88.5	-82.7	-103.3
BG14	$\text{Ga}(\text{C}_2\text{H}_5) + \text{C}_2\text{H}_5\cdot \rightarrow \text{GaC}_2\text{H}_4\cdot + \text{C}_2\text{H}_6$	-40.4	-27.8	-26.3	-23.7	-34.6	-17.7	-15.8	-12.4	-38.4
BG15	$\text{Ga}(\text{C}_2\text{H}_5)_3 + \text{H}_2 \rightarrow \text{Ga}(\text{C}_2\text{H}_5)_2\text{H} + \text{C}_2\text{H}_6$	-39.6	-56.3	-59.1	-63.6	-30.5	-26.2	-26.0	-25.2	-37.6
BG16	$\text{Ga}(\text{C}_2\text{H}_5)_2\text{H} + \text{H}_2 \rightarrow \text{Ga}(\text{C}_2\text{H}_5)\text{H}_2 + \text{C}_2\text{H}_6$	-38.8	-30.2	-29.2	-27.1	-31.7	-28.0	-27.9	-27.3	-38.6
BG17	$\text{Ga}(\text{C}_2\text{H}_5)\text{H}_2 + \text{H}_2 \rightarrow \text{GaH}_3 + \text{C}_2\text{H}_6$	-37.7	-37.6	-37.9	-38.0	-32.9	-31.8	-32.1	-32.2	-39.5
BG18	$\text{Ga}(\text{C}_2\text{H}_5) + \text{H}_2 \rightarrow \text{GaH} + \text{C}_2\text{H}_6$	-31.9	-21.9	-21.0	-19.1	-25.5	-15.7	-14.9	-13.3	-30.1
BG19	$\text{Ga}(\text{C}_2\text{H}_5)_2\cdot + \text{H}_2 \rightarrow \text{Ga}(\text{C}_2\text{H}_5)\text{H}\cdot + \text{C}_2\text{H}_6$	-35.7	-31.9	-31.5	-30.4	-30.3	-20.0	-18.8	-16.3	-37.1

Table 3. Unimolecular decomposition reactions of TBP and related products. Changes in electronic (ΔE) and Gibbs energy (ΔG) for temperatures of 400 °C (a), 500 °C (b) and 675 °C (c) are given in kJ mol^{-1} . Mechanisms are grouped as homolytical bond cleavages (AP1 - AP5), β -hydrogen eliminations (AP6 - AP7), alkane eliminations (AP8 - AP9) and H_2 eliminations (AP10 - AP12).

Reaction index	Reaction scheme	PBE-D3/TZ				MP2/TZ				CCSD(T)/TZ
		ΔE	ΔG a)	ΔG b)	ΔG c)	ΔE	ΔG a)	ΔG b)	ΔG c)	ΔE
AP1	$\text{P}(t\text{-C}_4\text{H}_9)\text{H}_2 \rightarrow \text{P}(t\text{-C}_4\text{H}_9)\text{H}\cdot + \text{H}\cdot$	349.7	230.9	215.5	188.3	352.2	231.6	216.0	188.6	357.4
AP2	$\text{P}(t\text{-C}_4\text{H}_9)\text{H}_2 \rightarrow \text{PH}_2\cdot + t\text{-C}_4\text{H}_9\cdot$	279.3	119.9	99.1	62.9	314.4	156.6	135.8	99.8	289.2
AP3	$\text{P}(t\text{-C}_4\text{H}_9)\text{H}\cdot \rightarrow \text{PH} + t\text{-C}_4\text{H}_9\cdot$	266.1	126.6	108.0	75.8	281.4	143.7	125.3	93.2	260.7
AP4	$\text{PH}_3 \rightarrow \text{H}_2\text{P}\cdot + \text{H}\cdot$	356.9	239.9	224.8	198.2	353.3	234.6	219.4	192.7	360.1
AP5	$\text{PH} \rightarrow \text{P}\cdot + \text{H}\cdot$	313.8	218.9	205.6	181.9	277.6	181.6	168.2	144.4	295.8
AP6	$\text{P}(t\text{-C}_4\text{H}_9)\text{H}_2 \rightarrow \text{PH}_3 + i\text{-C}_4\text{H}_8$	96.9	-48.7	-67.6	-100.5	111.7	-36.3	-55.7	-89.3	96.3
AP7	$\text{P}(t\text{-C}_4\text{H}_9) \rightarrow \text{PH} + i\text{-C}_4\text{H}_8$	111.4	-20.8	-38.0	-67.9	114.1	-21.4	-39.1	-69.9	100.9
AP8	$\text{P}(t\text{-C}_4\text{H}_9)\text{H}_2 \rightarrow \text{PH} + i\text{-C}_4\text{H}_{10}$	205.9	90.6	73.3	46.2	199.0	81.6	65.0	36.3	184.4
AP9	$\text{P}(t\text{-C}_4\text{H}_9)\text{H}\cdot \rightarrow \text{P}\cdot + i\text{-C}_4\text{H}_{10}$	170.0	78.7	64.5	39.8	124.5	31.7	17.2	-7.8	122.8
AP10	$\text{P}(t\text{-C}_4\text{H}_9)\text{H}_2 \rightarrow \text{P}(t\text{-C}_4\text{H}_9) + \text{H}_2$	239.9	123.2	107.4	79.9	236.8	119.0	103.1	75.5	231.0
AP11	$\text{PH}_3 \rightarrow \text{PH} + \text{H}_2$	254.5	151.1	137.1	112.5	239.2	133.9	119.7	94.9	235.7
AP12	$\text{PH}_2\cdot \rightarrow \text{P}\cdot + \text{H}_2$	211.5	130.2	117.9	96.1	163.5	80.9	68.5	46.7	171.4

Table 4. Bimolecular decomposition reactions of TBP and related products. Changes in electronic (ΔE) and Gibbs energy (ΔG) for temperatures of 400 °C (a), 500 °C (b) and 675 °C (c) are given in kJ mol^{-1} . Mechanisms are grouped as alkane/alkene and/or H_2 eliminations with $\text{H}\cdot$ (BP1 - BP5), ${}^t\text{C}_4\text{H}_9\cdot$ (BP6) or H_2 (BP7 - BP12) as reaction partner.

Reaction index	Reaction scheme	PBE-D3/TZ				MP2/TZ				CCSD(T)/TZ
		ΔE	ΔG a)	ΔG b)	ΔG c)	ΔE	ΔG a)	ΔG b)	ΔG c)	ΔE
BP1	$\text{P}(t\text{-C}_4\text{H}_9)\text{H}_2 + \text{H}\cdot \rightarrow \text{P}(t\text{-C}_4\text{H}_9)\text{H}\cdot + \text{H}_2$	-89.1	-95.5	-96.7	-98.6	-81.1	-87.8	-89.2	-91.2	-96.0
BP2	$\text{P}(t\text{-C}_4\text{H}_9)\text{H}_2 + \text{H}\cdot \rightarrow \text{PH}_2\cdot + i\text{-C}_4\text{H}_{10}$	-130.6	-147.0	-150.1	-154.9	-120.1	-137.1	-140.5	-145.8	-144.6
BP3	$\text{P}(t\text{-C}_4\text{H}_9) + \text{H}\cdot \rightarrow \text{P}\cdot + i\text{-C}_4\text{H}_{10}$	-159.0	-140.0	-139.6	-138.7	-193.4	-175.2	-175.1	-174.6	-204.2
BP4	$\text{PH}_3 + \text{H}\cdot \rightarrow \text{PH}_2\cdot + \text{H}_2$	-81.9	-86.5	-87.3	-88.6	-80.0	-84.8	-85.7	-87.1	-93.4
BP5	$\text{PH} + \text{H}\cdot \rightarrow \text{P}\cdot + \text{H}_2$	-125.0	-107.4	-106.6	-105.0	-155.7	-137.8	-136.9	-135.4	-157.7
BP6	$\text{P}(t\text{-C}_4\text{H}_9)\text{H}_2 + {}^t\text{C}_4\text{H}_9\cdot \rightarrow \text{P}(t\text{-C}_4\text{H}_9)\text{H}\cdot + i\text{-C}_4\text{H}_{10}$	-60.2	-36.0	-33.7	-29.6	-82.4	-62.1	-60.3	-57.0	-76.3
BP7	$\text{P}(t\text{-C}_4\text{H}_9)\text{H}_2 + \text{H}_2 \rightarrow \text{PH}_3 + i\text{-C}_4\text{H}_{10}$	-48.6	-60.5	-62.8	-66.3	-40.2	-52.3	-54.8	-58.7	-51.2
BP8	$\text{P}(t\text{-C}_4\text{H}_9)\text{H}_2 + \text{H}_2 \rightarrow \text{PH}_3 + i\text{-C}_4\text{H}_8 + \text{H}_2$	96.9	-48.7	-67.6	-100.5	111.7	-36.3	-55.7	-89.3	96.7
BP9	$\text{P}(t\text{-C}_4\text{H}_9)\text{H}\cdot + \text{H}_2 \rightarrow \text{P}\cdot + i\text{-C}_4\text{H}_{10}$	-41.5	-51.5	-53.4	-56.3	-39.0	-49.2	-51.3	-54.5	-48.6
BP10	$\text{P}(t\text{-C}_4\text{H}_9) + \text{H}_2 \rightarrow \text{PH} + i\text{-C}_4\text{H}_{10}$	-34.1	-32.6	-33.1	-33.7	-37.8	-37.4	-38.2	-39.3	-46.5

Table 5. Transition state data for selected decomposition reactions of TEG, TBP and related products at PBE-D3/TZ. Electronic energies of activation (ΔE^\ddagger) and Gibbs energy of activation (ΔG^\ddagger) for temperatures of 400 °C (a), 500 °C (b) and 675 °C (c) are given in kJ mol^{-1} . The transition states' imaginary vibrational mode (ν_{imag}) is given in cm^{-1} . Reactions AG11 - AG14 and AP6 represent unimolecular β -hydrogen, AG15 - AG17 and AG19 - AG20 represent unimolecular alkane and H_2 eliminations, respectively. BG15 - BG19 and BP8 represent bimolecular alkane and H_2 eliminations, respectively.

Reaction index	Reaction scheme	ΔE^\ddagger	ΔG^\ddagger a)	ΔG^\ddagger b)	ΔG^\ddagger c)	ν_{imag}	ΔE^\ddagger MP2/TZ //PBE-D3/TZ[a]	ΔE^\ddagger CCSD(T)/TZ //PBE-D3/TZ[a]
AG11	$\text{Ga}(\text{C}_2\text{H}_5)_3 \rightarrow \text{Ga}(\text{C}_2\text{H}_5)_2\text{H} + \text{C}_2\text{H}_4$	131.6	141.0	144.3	150.2	i648	152.6	147.5
AG12	$\text{Ga}(\text{C}_2\text{H}_5)_2\text{H} \rightarrow \text{Ga}(\text{C}_2\text{H}_5)\text{H}_2 + \text{C}_2\text{H}_4$	128.1	149.9	155.1	164.2	i686	150.7	145.3
AG13	$\text{Ga}(\text{C}_2\text{H}_5)\text{H}_2 \rightarrow \text{GaH}_3 + \text{C}_2\text{H}_4$	123.8	129.2	131.9	136.7	i717	149.6	143.3
AG14	$\text{Ga}(\text{C}_2\text{H}_5) \rightarrow \text{GaH} + \text{C}_2\text{H}_4$	87.2	82.6	84.1	86.8	i430	111.5	109.7
AG15	$\text{Ga}(\text{C}_2\text{H}_5)_3 \rightarrow \text{Ga}(\text{C}_2\text{H}_5) + n\text{-C}_4\text{H}_{10}$	312.3	326.2	329.4	335.1	i377	375.3	360.1
AG17	$\text{Ga}(\text{C}_2\text{H}_5)\text{H}_2 \rightarrow \text{HGa} + \text{C}_2\text{H}_6$	194.7	199.8	202.2	206.7	i713	234.2	236.9
AG19	$\text{Ga}(\text{C}_2\text{H}_5)\text{H}_2 \rightarrow \text{Ga}(\text{C}_2\text{H}_5) + \text{H}_2$	217.0	215.6	216.8	219.1	i1140	271.2	255.7
AG20	$\text{GaH}_3 \rightarrow \text{HGa} + \text{H}_2$	211.5	200.5	200.5	200.4	i1025	269.0	251.4
BG15	$\text{Ga}(\text{C}_2\text{H}_5)_3 + \text{H}_2 \rightarrow \text{Ga}(\text{C}_2\text{H}_5)_2\text{H} + \text{C}_2\text{H}_6$	96.7	208.5	225.2	254.5	i1233	126.2	124.7
BG16	$\text{Ga}(\text{C}_2\text{H}_5)_2\text{H} + \text{H}_2 \rightarrow \text{Ga}(\text{C}_2\text{H}_5)\text{H}_2 + \text{C}_2\text{H}_6$	93.7	217.0	235.4	267.6	i1258	124.3	122.8
BG17	$\text{Ga}(\text{C}_2\text{H}_5)\text{H}_2 + \text{H}_2 \rightarrow \text{GaH}_3 + \text{C}_2\text{H}_6$	92.1	204.7	221.5	251.0	i1283	124.3	122.6
BG18	$\text{Ga}(\text{C}_2\text{H}_5) + \text{H}_2 \rightarrow \text{GaH} + \text{C}_2\text{H}_6$	67.3	169.2	184.8	212.0	i1156	105.4	107.3
AP6	$\text{P}(t\text{-C}_4\text{H}_9)\text{H}_2 \rightarrow \text{PH}_3 + i\text{-C}_4\text{H}_8$	242.6	217.4	216.2	214.1	i648	310.5	293.1
BP8	$\text{P}(t\text{-C}_4\text{H}_9)\text{H}_2 + \text{H}_2 \rightarrow \text{PH}_3 + i\text{-C}_4\text{H}_8 + \text{H}_2$	264.6	337.3	350.1	372.4	i1120	365.8	354.0

[a] Energy calculations based on PBE-D3/TZ structures.

Table 6. Statistical deviation of PBE-D3/TZ and MP2/TZ reaction energies (ΔE) w.r.t. CCSD(T)/TZ energies and barriers (ΔE^\ddagger) w.r.t. CCSD(T)/TZ and MP2/TZ energies. *Method1//method2* indicates an energy calculation by *method1* on the structure optimized with *method2*.

	Reaction energies						Reaction barriers	
	PBE-D3 w.r.t. CCSD(T)//MP2			MP2 w.r.t. CCSD(T)//MP2			PBE-D3 w.r.t. CCSD(T)// PBE-D3	PBE-D3 w.r.t. MP2// PBE-D3
	all	radicals	non-rad.	all	radicals	non-rad.	all	all
RMS ^[a]	17.7	19.5	13.6	14.4	15.8	11.0	40.8	48.7
MAE ^[b]	-47.2	-47.2	42.4	-40.6	-40.6	-17.7	89.5	101.2
RAD ^[c]	12.0	12.0	11.9	12.0	10.3	14.4	20.4	22.3
RMD ^[d]	-38.5	-38.5	24.9	-25.9	-19.3	-25.9	37.3	36.2

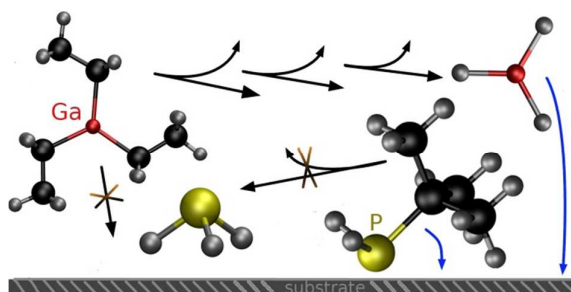
[a] Root mean square error in kJ mol^{-1} .

[b] Maximum absolute error in kJ mol^{-1} .

[c] Relative average deviation in %.

[d] Relative maximum deviation in %.

Graphical Table of Content



Gas phase decomposition products of MOVPE precursor molecules TEG and TBP were identified via thermodynamic and kinetic data from a catalogue of 61 elementary reactions as calculated by quantum chemical methods.